Journal of Building Engineering 76 (2023) 107125

Contents lists available at ScienceDirect

Journal of Building Engineering

journal homepage: www.elsevier.com/locate/jobe

Image-based 3D modeling-to-simulation of single-wythe masonry structure via reverse descriptive geometry

Mohammad Abu-Haifa [a], Seung Jae Lee [a,*]

[a] Department of Civil and Environmental Engineering, Florida International University, Miami, FL, USA

ARTICLE INFO

Keywords:
Single-wythe masonry structures
Descriptive geometry
Image processing
Image-based 3D modeling-to-simulation
Discrete element method (DEM)
Impulse-based dynamic simulation

ABSTRACT

This study aims to develop an innovative image-based 3D modeling-to-simulation framework that can efficiently assess the hazard vulnerability of single-wythe masonry structures. Using the novel concept of 'reverse descriptive geometry', the framework utilizes 2D masonry wall images to model a 3D single-wythe masonry structure, subsequently converting it into a 3D discrete element model for the vulnerability assessment. The methodology involves segmenting all bricks in the 2D images, identifying the brick geometries by tracing the boundaries, and approximating those into polygons using the splitting method. By incorporating the wall orientations, the simplified 2D polygons are introduced into 3D space and subsequently extruded to a specified thickness. The corners between the walls, i.e., adjoining wythes, are realistically modeled with a type of structural masonry bond. The digitally constructed 3D masonry geometry is enriched with physical properties such as brick mass and mortar strengths, enabling a seamless 3D discrete element simulation to gauge the hazard vulnerability. The proposed framework is successfully applied to Stylite Tower, a heritage single-wythe masonry structure in Jordan. The results demonstrate a remarkable geometric accuracy achieved and further illustrate the structure's potential vulnerability under seismic events, highlighting the efficiency and efficacy of the developed framework. This study introduces a streamlined procedure leveraging a single 2D image per wall for 3D modeling of a structure, thus highly efficient. A discrete element modeling is adopted instead of finite element methods based on a continuum theory. Therefore, this approach accurately captures the discontinuous nature of masonry structures, resulting in a high fidelity in simulation. Furthermore, this study adopts an impulse-based dynamic simulation method that is far more computationally efficient and tolerant to geometric errors than the conventional discrete element method. Therefore, the proposed framework presents a significant advancement in the vulnerability assessment of masonry structures, providing a novel, efficient, and reliable methodology for engineering practice.

1. Introduction

Masonry structures constitute a significant sub-population of the historic heritage, and make up the largest proportion of the building stock worldwide [1]. Single-wythe masonry structures are constructed with walls of one masonry unit thickness, thus the masonry wall serves as both a structural system and an exterior facing. Many masonry structures have been constructed as unreinforced single-wythe structures due to the lower construction cost, convenience of maintenance and reasonable structural stability [2].

* Corresponding author.
E-mail addresses: mabuh004@fiu.edu (M. Abu-Haifa), sjlee@fiu.edu (S.J. Lee).

https://doi.org/10.1016/j.jobe.2023.107125
Received 31 January 2023; Received in revised form 14 June 2023; Accepted 15 June 2023
Available online 21 June 2023

For example, single-wythe masonry structures make up around 8% of all masonry structures in Sicily, Italy [3]. In the 1990s, the price of wood increased [4], leading to an increase in the popularity of single-wythe load bearing masonry walls [5], and those are still widely used these days due to the cost competitiveness. However, these single-wythe masonry structures are more vulnerable to hazards than multi-wythe structures [6]. Many heritage masonry structures are single-wythe, and many of them have been severely damaged or are exposed to various hazards such as strength degradation, vibration caused by nearby traffic, wind and earthquakes, lack of maintenance, vandalism, etc. [1,7]. With its enormous value as heritage, it is of great importance to estimate the aggravating impact of these hazards on single-wythe masonry structures to better identify the preservation needs and preventive measures for damage mitigation.

Experimental investigations have been conducted on single-wythe masonry structures to estimate their vulnerability to various hazards including seismic performance, blast-induced loadings, axial compression and shear loading, traffic-induced vibration, and the impact of wind driven rain [8–15]. However, experimental studies on heritage single-wythe masonry structures have limitations in robustly estimating overall structural performance depending on the required test and structure size [16]. Therefore, numerical analysis has been adopted in the research community as an alternative approach [16–18].

Numerical modeling of masonry structures can be conducted using two different approaches: continuum- or discontinuum-based methods. These approaches aim to model the mechanical behavior of the structures at either macro- or micro-scale, respectively [19]. The continuum-based approach, such as the finite element method (FEM), models the whole masonry structure as a continuous medium. Therefore, the structural behavior after the onset of failure may not be realistic [20]. On the other hand, the discontinuum-based approach, such as the discrete element method (DEM), simulates the discontinuous nature of masonry bricks by explicitly modeling the individual bricks and their interactions [7]. Therefore, DEM has been broadly adopted to investigate the behavior of masonry structures in the research community [20–30].

Nevertheless, discrete element modeling for large heritage single-wythe masonry structures is considered a difficult task [26]. A masonry structure may contain too many bricks to be modeled manually. Furthermore, a lot of those structures are rubble masonry, where the stone bricks have a non-rectangular shape. Therefore, manual discrete element modeling of these masonry structures may be

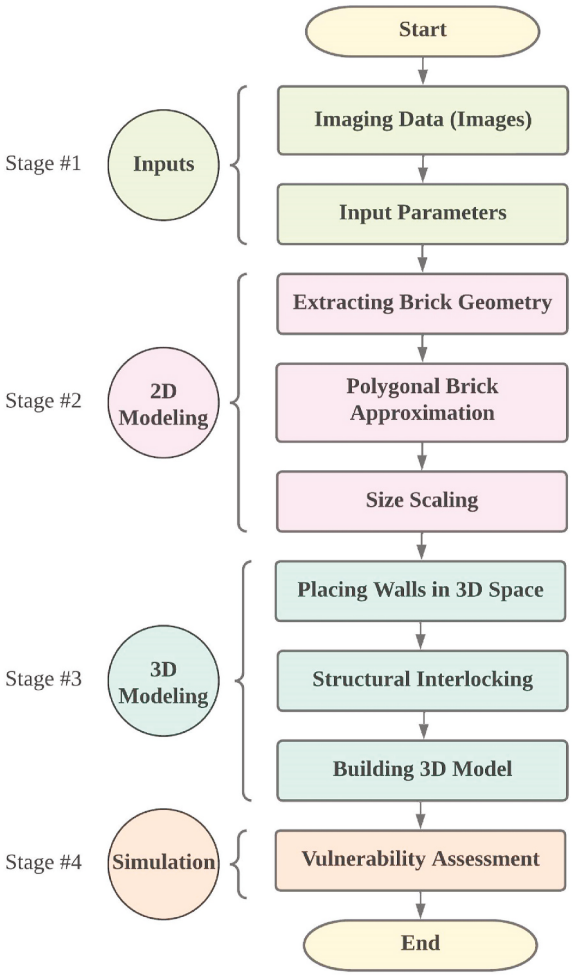

Fig. 1. Overview of the proposed streamlined image-based 3D modeling-to-simulation framework for single-wythe masonry structures.

impractical and sometimes infeasible. The accuracy of the DEM simulation of masonry structures is also limited without the brick shapes being accurately modeled. To overcome these challenges, imaging techniques have been recently adopted to capture the ground truth brick geometry [26,31–36]. For example, an innovative framework has been developed to use a single masonry image for streamlined image-based DEM modeling [31], but this approach is limited to the modeling of a planar masonry wall. A framework that converts a large set of images into a whole 3D masonry structure of multiple walls has been proposed [26]. While this study provided great insights, this method did not consider the actual geometry of brick shapes due to its voxelization of the masonry structure.

The objective of this paper is to develop a streamlined image-based 3D modeling-to-simulation framework for the discrete element analysis of single-wythe masonry structures that will make valuable contributions to masonry preservation and diagnostics. By efficiently converting visual data (images) into actionable knowledge, this research aims to enhance the assessment of structural vulnerability and facilitate the implementation of preventive measures for mitigating potential risks and damages in single-wythe masonry structures. This paper is built upon the authors' previous work presented in Ref. [31] that focused on a planar masonry wall. The main difference from the previous work is the use of 'reverse descriptive geometry' that adopts a set of 2D wall images to digitally construct a 3D masonry structure model composed of multiple walls. One photographic image for each wall is needed for the 2D-to-3D modeling. The modeled 3D masonry structure is then used for DEM analysis. The provided framework presents an integrated approach that incorporates image analysis, numerical modeling, and simulation methods to systematically assess the hazard vulnerability of single-wythe masonry structures. This comprehensive, cost-effective, and efficient approach aims to enhance the practice of risk assessment, allowing for a more accurate estimation of the structures' vulnerability under different hazard scenarios. By implementing this approach, the resilience and preservation of single-wythe heritage masonry structures can be effectively enhanced. Section 2 introduces the proposed framework and demonstrates it using a virtual masonry structure as an example. In Section 3, this approach is specifically applied to a heritage single-wythe masonry structure.

2. Methodology

The core of the proposed framework in this paper is a 2D-to-3D approach, which may be considered as an opposite concept of the conventional descriptive geometry (also known as the stereotomy) that represents a 3D object with multiple 2D geometric projections, i.e., 3D-to-2D [37]. The proposed framework uses the novel concept of 'reverse descriptive geometry' whereby the 2D projection images are used to digitally construct a 3D object.

An overview of the streamlined image-based 3D modeling-to-simulation framework for single-wythe masonry structures is presented in Fig. 1, where the framework is divided into four stages and several steps in each stage: 1) Input acquisition – the 2D planar masonry wall images are obtained along with other identified input parameters; 2) 2D modeling – a set of 2D planar masonry wall models is developed from each 2D masonry wall image; 3) 3D modeling – in this stage, the 2D planar masonry wall models are introduced in a 3D space and extruded. The adjoining wythes at the building corners are constructed, taking account of a structural masonry bond pattern; and 4) Simulation – the 3D masonry model is simulated using DEM to estimate the hazard vulnerability of the structure. MATLAB [38] is used to develop the bespoke codes to automate the imaging-to-simulation process. It is worth noting that the developed image-based modeling process is fully automatic. Once the binary images of the walls are obtained and the input parameters are identified, the algorithm automatically builds the whole 3D DEM model of the structure. A free and open-source 3D computer graphics software, Blender [39], and its integrated Bullet physics engine [40] are used for DEM simulation of 3D masonry structures. The Bullet physics engine works on the impulse-based dynamic simulation that can be seen as a momentum-exchange method, which is a DEM [41].

An example single-wythe masonry structure shown in Fig. 2 is used in Section 2 to illustrate the procedures in the proposed framework. The model has six sides (walls), where each wall has a different height and width. The structure is composed of typical rectangular bricks with a size of 400 × 180 × 180 mm (width × depth × height), and a 10 mm mortar layer in-between. All walls are

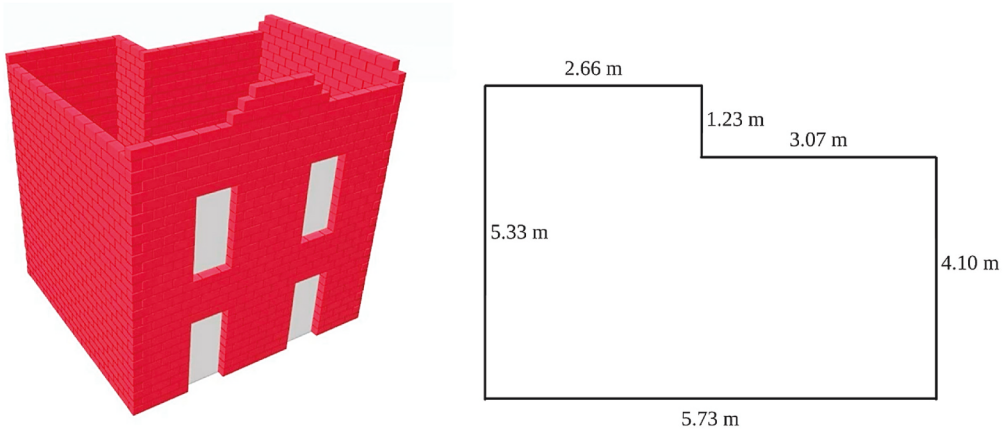

Fig. 2. Virtual 3D single-wythe masonry structure as an example to demonstrate the image-based 3D modeling-to-simulation framework, where the dimensions are shown on the plan view.

nearly half-brick thick. There is no particular reason for selecting the brick size, as the proposed method will work with any brick size. That being said, the chosen brick resembles the dimensions of the 8-inch thru-wall double monarch brick. The stretcher bond type is considered at the adjoining wythe, which is widely used for half-brick masonry walls [42]. Stretcher bond is a repeating pattern in which each layer alternates with an offset of half a brick, preventing a straight joint across the layers [43].

2.1. Inputs (stage 1)

2.1.1. Input images

One image for each side of the structure is going to be used as input for the modeling. The images may be stitched or cut to represent a wall in one image. Fig. 3 presents all the input images for the example single-wythe masonry structure, in which each image represents a wall of the structure.

2.1.2. Input parameters

The framework requires four input parameters as well as the input wall images: (i) dimension (width and height) of walls, (iii) orientation of walls, (iv) brick thickness, and (v) target number of vertices to represent each brick in modeling. The images are to be numbered in ascending order, starting from the front wall and moving counterclockwise as in Fig. 3, where the wall images are numbered from 1 to 6. Table 1 shows the input parameters and their corresponding values. The orientation of the wall is determined counterclockwise from the global coordinate system (i.e., the global X-axis). In this paper, X, Y, and Z refer to the global coordinates. For the example structure, the origin of the global coordinate system is set at the lower-left corner of the front wall (i.e., wall #1) as in Fig. 4, and the orientation θ of all images (walls) can be defined counterclockwise as shown in Table 1. As a note, a target accuracy level can be used (instead of the target number of vertices) as an input to ensure the minimum accuracy required to represent all bricks. For simplicity, however, this study adopts the same number of vertices to represent all bricks, resulting in each brick being modeled with different accuracies.

2.2. 2D wall modeling (stage 2)

2.2.1. Extracting brick geometry

Image segmentation is required to distinguish bricks from mortar and to extract the brick geometries. Image segmentation is the process of translating a digital image into smaller meaningful subclasses or objects for further analysis of the image [44]. Technically, the process labels every pixel in the image based on certain characteristics such as intensity, color, and texture. However, manual segmentation is time-consuming and impractical, considering a masonry structure may contain too many bricks to segment. Various automatic and semi-automatic algorithms were developed to facilitate this process [45–47]. The segmentation output is a converted black and white binary image, where the bricks can be represented as white pixels and the mortar is represented as black pixels. This study adopts the segmentation approach adopted by Ref. [31]. The segmented wall images are shown in Fig. 5, where the segmented bricks are colored randomly to illustrate that each brick is identified as an individual object.

While segmented, the bricks in the image are not polygons yet. To this end, the MATLAB boundary tracing function [48] is used to extract the geometry of each brick and present it as a polygon. The boundary of each segmented brick is traced, from which the boundary pixel locations are identified. The bricks are then converted into a set of polygons, where each boundary pixel is used to create the vertices of the polygon. This process typically results in polygons with a large number of vertices because each brick in a segmented image is represented by many pixels. Table 2 shows the average number of vertices that represent each brick polygon, for which about 200 vertices are used. The average number of vertices is calculated by dividing the sum of V_j by k, where V_j is the number of vertices representing brick j in a wall and k is the number of bricks in the wall.

2.2.2. Polygon brick approximation

Modeling a simple brick shape (e.g., a rectangle) with a polygon with about 200 vertices is clearly inefficient. Therefore, this step converts the polygons into simpler ones by eliminating redundant vertices, for which this study adopts the splitting method [49]. By

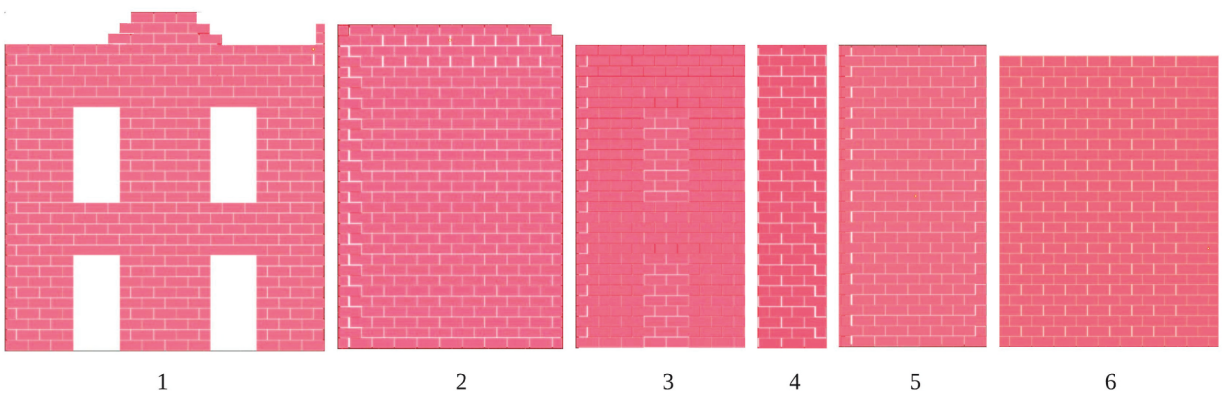

Fig. 3. Input images from all sides of the example single-wythe masonry structure (shown with the image numbers).

Table 1
Input parameters considered for the example single-wythe masonry structure.

Wall				Brick thickness (m)	Target number of vertices
Image n	Width W_n (m)	Height H_n (m)	Orientation θ_n (°)		
1	5.73	6.07	0	0.18	5
2	4.10	5.88	90	0.18	5
3	3.07	5.50	180	0.18	5
4	1.23	5.50	90	0.18	5
5	2.66	5.50	180	0.18	5
6	5.33	5.31	270	0.18	5

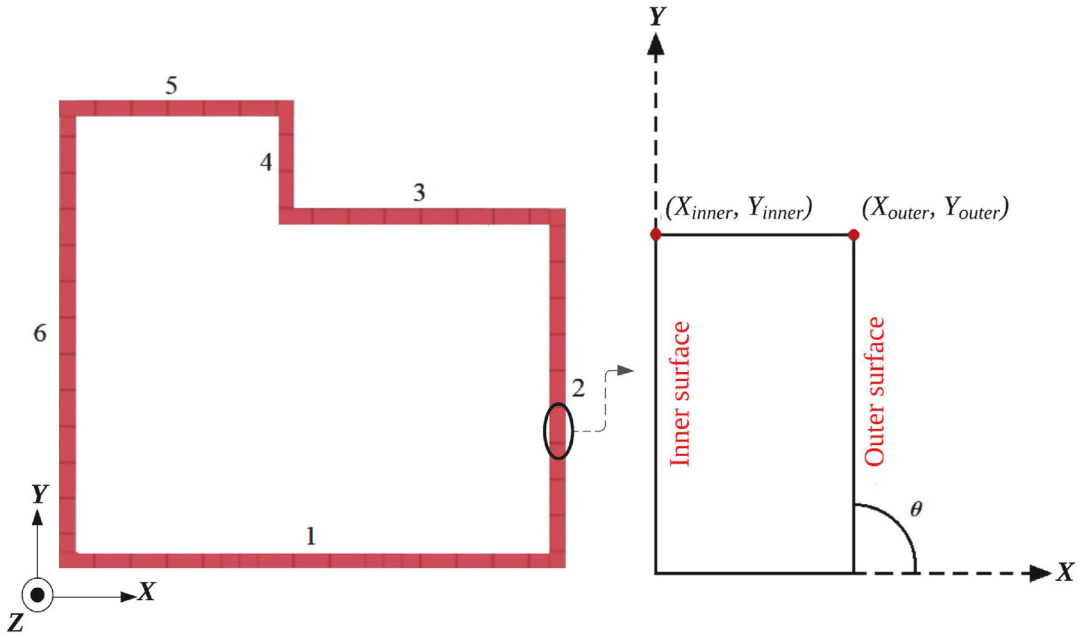

Fig. 4. Plan view of the example single-wythe masonry structure; X, Y, and Z refer to the global coordinates.

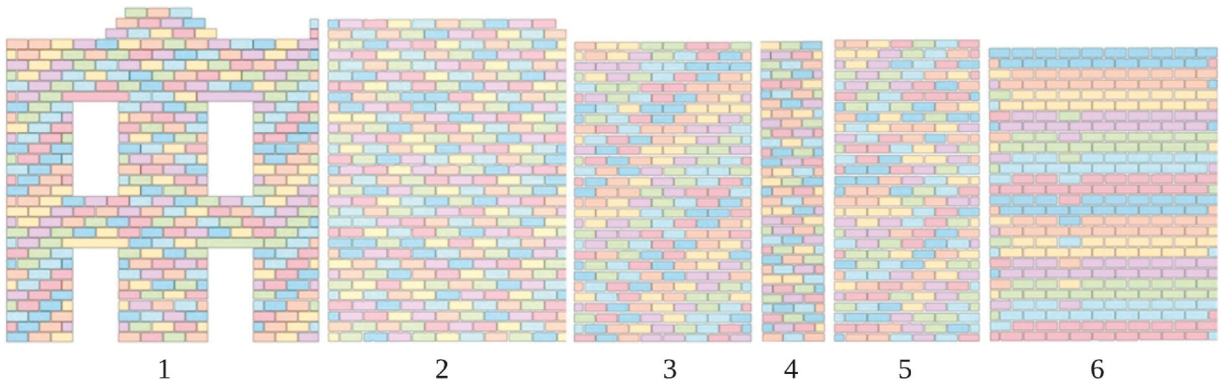

Fig. 5. Segmentation results for the input images of the virtual single-wythe masonry structure.

identifying a line that connects the two farthest points on the boundary, the splitting method iteratively splits the shape into two halves. The points that have the maximum perpendicular distance from the line are identified, forming the four boundary vertices. Virtual lines are built between these vertices, and the process is repeated until the polygon is simplified to the desired number of vertices. In the end, the simplified polygon is drawn by connecting the final vertices with lines.

Hypothetically, four vertices would be enough to represent the rectangular brick shape in the example structure, but a few more vertices would be helpful to account for some geometric variation in brick shapes [50]. Fig. 6 shows an example. The brick polygon in

Table 2
Average number of vertices to represent each brick polygon in all walls.

Wall image #	Average number of vertices for each brick polygon
1	237.37
2	235.94
3	186.59
4	220.90
5	184.14
6	234.08

Fig. 6a obtained from a segmented image is approximately rectangular, but not in an exact sense. Fig. 6b and c present brick polygons approximated with 4 and 5 vertices, respectively. Clearly, Fig. 6c better represents the overall shape than Fig. 6b, where the geometric variation is accounted for. A MATLAB code [51] is employed to simplify polygon shapes in all walls.

2.2.3. Size scaling

The image coordinates are defined in pixels and have their origin at the upper-left corner for the width (w) and height (h) of the wall image. Accordingly, the locations of all brick polygons inside a wall are defined in pixels. Therefore, the pixel-based coordinates need to be translated to a local Cartesian coordinate system, where the origin is at the lower-left corner of each wall, as shown in Fig. 7. Please note that the lower cases (x, y, and z) are used to indicate the local coordinate system, compared to the upper cases for the global coordinate system (as discussed in Section 2.1.2). The y coordinate is 0 as it is a 2D image. In this step, the coordinates of each vertex are scaled based on the actual wall dimensions (which are input parameters) from pixels to a physical length, e.g., meters. The x- and z-coordinates are scaled by the width and height ratios (W/w) and (H/h), respectively, where W and H are the actual wall width and height (as in Table 1). Then, the pixel-based z-coordinate is subtracted from H to convert it into the Cartesian coordinate with the origin at the lower left corner of the wall, as shown in Eq. (1). The z_{pixel} and $z_{Cartesian}$ represent z coordinates in pixel and Cartesian-based coordinates, respectively.

$$z_{Cartesian} = H - z_{pixel} \times \frac{H}{h} \tag{1}$$

2.3. 3D structure modeling (stage 3)

This stage constructs the 3D model of the single-wythe masonry structure based on the processed data obtained from the previous stage (i.e., 2D modeling) to build the whole 3D DEM masonry model.

2.3.1. Placing walls in 3D space

This step places the 2D walls (in local coordinates) into 3D space (in global coordinates), for which the relationship between the local and global coordinates is developed using a rotation matrix as in Eq. (2). The Z-coordinate (global) equals its z-coordinate (local), and the y-coordinate (local) is always 0, so Eq. (2) can be simplified to Eq. (3). Please note that the subscript *outer* denotes the coordinates of the brick surface facing 'outward', while the subscript *inner* is reserved for a later step to indicate the coordinates of the brick surface facing 'inward' (see Fig. 4) after the walls are extruded in the thickness direction (to be discussed in Section 2.3.3). Per user input, θ is the angle between the X-axis and x-axis of a wall, n is the wall number to compute the global coordinates, and W_n is the width of wall n. Therefore, $(X_{outer})_n$ denotes X-coordinates of the *outer* brick surface in the n-th wall. For wall #1, $n = 1$ (thus no summation is needed), and θ_1 is 0 (thus global X and local x coordinates coincide, while the Y coordinates are all 0). Once the global coordinates of all bricks are obtained, the wall surfaces of the structure can be constructed as in Fig. 8, where the brick polygons (in green) are presented with 5 vertices as stated earlier.

$$\begin{bmatrix} (X_{outer})_n \\ (Y_{outer})_n \end{bmatrix} = \begin{bmatrix} \cos\theta_n & -\sin\theta_n \\ \sin\theta_n & \cos\theta_n \end{bmatrix} \begin{bmatrix} (x_{outer})_n \\ (y_{outer})_n = 0 \end{bmatrix} + \begin{bmatrix} \sum_{i=1}^{n-1} (W_i \cos\theta_i) \\ \sum_{i=1}^{n-1} (W_i \sin\theta_i) \end{bmatrix} \tag{2}$$

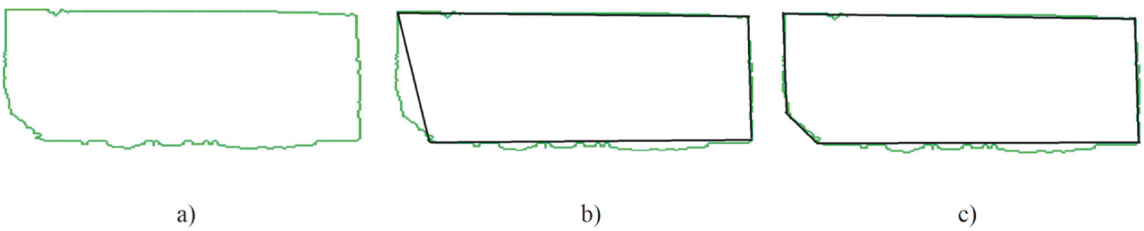

Fig. 6. Polygon brick approximation: (a) brick polygon obtained from segmented wall image; (b) polygon approximated with 4 vertices; and (c) polygon approximated with 5 vertices.

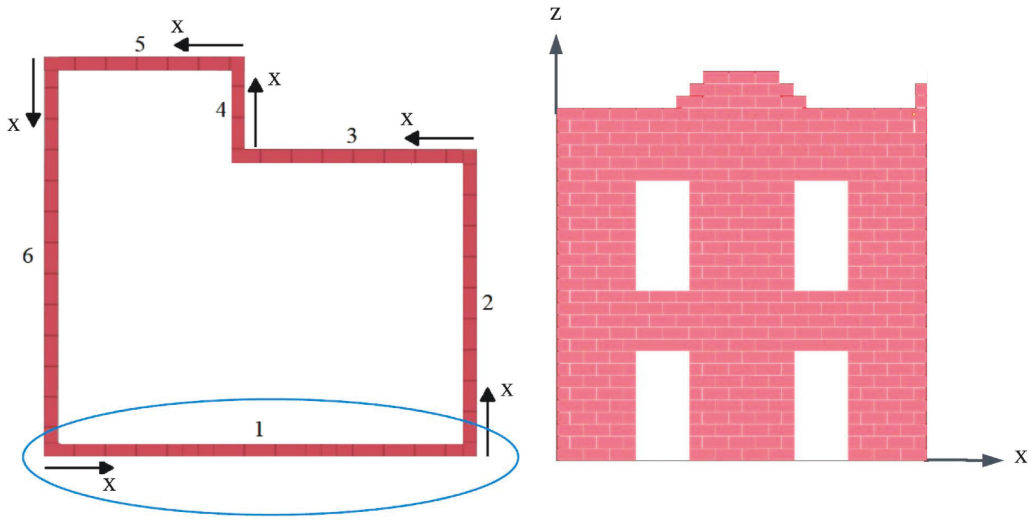

Fig. 7. Local coordinate system in terms of x and z in Cartesian coordinate system. Example shown with wall #1.

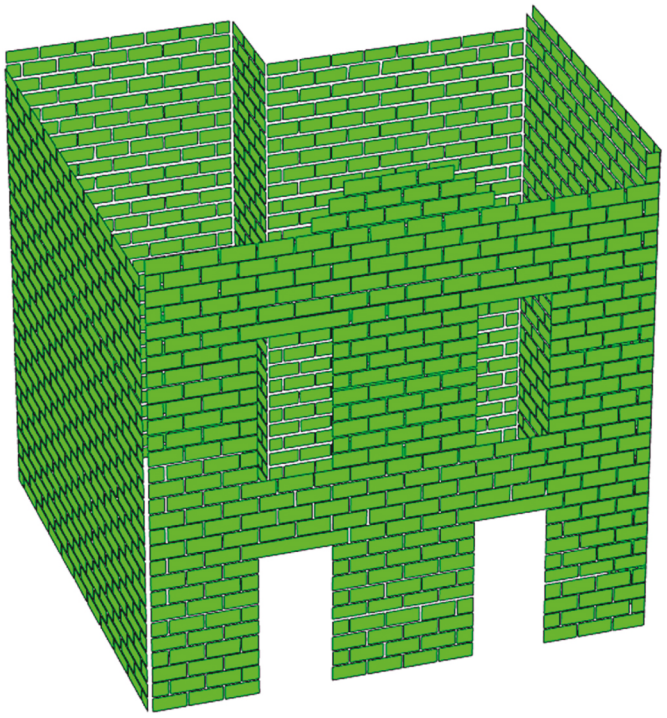

Fig. 8. The outer wall surfaces of the example single-wythe masonry structure.

$$\begin{bmatrix} (X_{outer})_n \\ (Y_{outer})_n \end{bmatrix} = \begin{bmatrix} (x_{outer})_n \cos\theta_n + \sum_{i=1}^{n-1} (W_i \cos\theta_i) \\ (x_{outer})_n \sin\theta_n + \sum_{i=1}^{n-1} (W_i \sin\theta_i) \end{bmatrix} \tag{3}$$

2.3.2. Structural interlocking

Stretcher bond is considered for adjoining wythes, i.e., structural masonry interlocking between walls. If all polygons in Fig. 8 are extruded in the thickness directions, overlapping occurs at the corners, as shown in Fig. 9. A solution to this is to remove one of the neighboring bricks at the adjoining wythes, e.g., if the red polygon in Fig. 9 is removed, then no overlapping would occur when the

remaining polygons in the neighbor are extruded. Therefore, polygons of a smaller size than a typical brick located at the corners are removed to properly model the stretcher bond.

Fig. 10 presents the flowchart to detect and remove the small polygons located at wall boundaries to model the stretcher bond. A threshold approach is adopted for this task [52]. It iteratively removes all polygons located between walls having an area approximately equal to a predefined threshold area (A_{th}). The area of a polygon and its center in the local coordinate system are determined. A corner polygon is detected if the *x*-coordinate of its center is approximately equal to half of the brick thickness ($t/2$) or located at the last half brick thickness of the wall width (W - $t/2$). All corner polygons having an approximately equal area to the threshold area are removed. Fig. 11 shows the wall surfaces of the example single-wythe masonry structure with these small corner polygons removed.

2.3.3. Building 3D model

A 3D brick polyhedron is created from each brick polygon after extruding it in the brick thickness direction. The *inner* wall coordinates can be found after the extrusion using Eq. (4), where t_n is the brick thickness of the *n*-th wall, which is entered as an input parameter. The *Z*-coordinate of any inner vertex is equal to its outer Z-coordinate ($Z_{inner} = Z_{outer}$). The 3D model of the single-wythe masonry structure is represented by 3D brick polyhedrons. The geometry of the 3D model is written in stereolithography (STL) file format.

$$\begin{bmatrix} (X_{inner})_n \\ (Y_{inner})_n \end{bmatrix} = \begin{bmatrix} \cos\theta_n & -\sin\theta_n \\ \sin\theta_n & \cos\theta_n \end{bmatrix} \begin{bmatrix} 0 \\ t_n \end{bmatrix} + \begin{bmatrix} (X_{outer})_n \\ (Y_{outer})_n \end{bmatrix} \tag{4}$$

2.4. DEM simulation (stage 4)

The 3D model is then used for DEM analysis of the building's vulnerability to hazards. Fig. 12 shows the developed 3D single-wythe masonry structure modeled with brick polyhedrons. Blender is used to conduct the DEM simulation of the modeled structure subjected to hazards. The Blender is a free and open-source 3D computer graphics software [39] that houses the Bullet physics engine [40] that simulates collisions between rigid bodies based on impulse-based dynamics. It is worth noting that numerical methods satisfying the following two requirements can be referred to as DEM per [53]: (1) allowing for finite displacements and rotations of discrete bodies, including complete separation of the bodies; and (2) automatically identifying new contacts as the simulation progresses. The momentum-exchange method is one of the four kinds of DEM that comply with this definition. The Bullet physics engine dynamically simulates rigid polyhedral bodies using an impulse-based dynamics scheme that can be considered as a momentum-exchange method [41]. The impulse-based dynamic simulation method (i.e., velocity-based) is computationally far more efficient than the conventional (i.e., force/acceleration-based) DEM, and it was reported to show a speed-up of almost two orders of magnitude with high simulation fidelity [55]. Therefore, the impulse-based dynamics approach is well suited for a large-scale simulation of many bricks. Furthermore, this approach is suitable for the image-based modeling-to-simulation of masonry structures due to its high tolerance for geometrical errors. The impulse-based dynamics approach considers relative velocity to resolve a collision between two bodies. Therefore, it has a greater tolerance for any penetration error that may be potentially caused by inaccurate image processing, e.g., influenced by lighting, shadow, image resolution, etc. On the other hand, the conventional DEM considers the relative position between two bodies (i.e., penetration) to resolve a collision (whereby the contact force is computed), which therefore any small geometrical error may trigger spurious energy gain and numerical instability in the modeled system. A Bullet plug-in, Bullet Constraints Builder (BCB), is used to model the mortar effect by setting constraints between adjacent bricks [54]. Constraints between bricks are aligned to the center-to-center line of both connected bricks. A detailed comparison between the conventional DEM and the impulse-based dynamic simulation method is provided in Ref. [55]. The constraint-based modeling of masonry structures is discussed in Ref. [31]. The mortar (constraint) between the bricks breaks once it reaches its breaking threshold. The breaking thresholds for the compressive, tensile, and shear strengths are used as the same values that were adopted in Ref. [31]. A synthetic magnitude 7 earthquake is applied for 10 s on the developed model. The collapse sequence of the modeled single-wythe masonry structure is realistically simulated, as shown in Fig. 13.

3. Application to a heritage single-wythe masonry structure

A real-world single-wythe masonry structure shown in Fig. 14 is considered as a case study to apply the developed image-based 3D modeling-to-simulation framework. The structure, known as Stylite Tower, is a heritage single-wythe masonry construction during the Byzantine period located at Umm ar-Rasas in Jordan, a UNESCO World Heritage Site. It is almost 13.5 m high [56], with a base dimension of 2.43 × 2.48 m. Stylite Tower is the only surviving tower of its kind in the world, thus it has enormous heritage value to preserve.

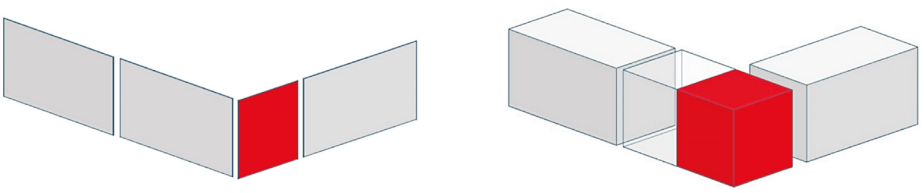

Fig. 9. Overlapping occurs when all polygons are extruded in the thickness directions.

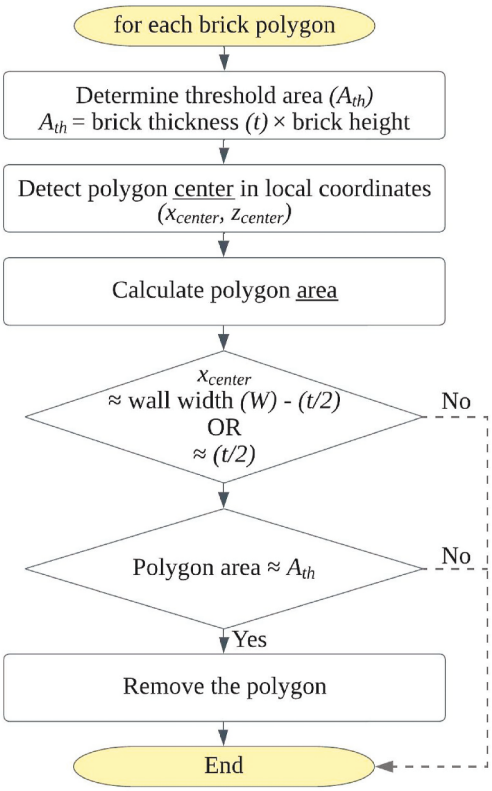

Fig. 10. Flowchart for the threshold method adopted to consider the stretcher bond.

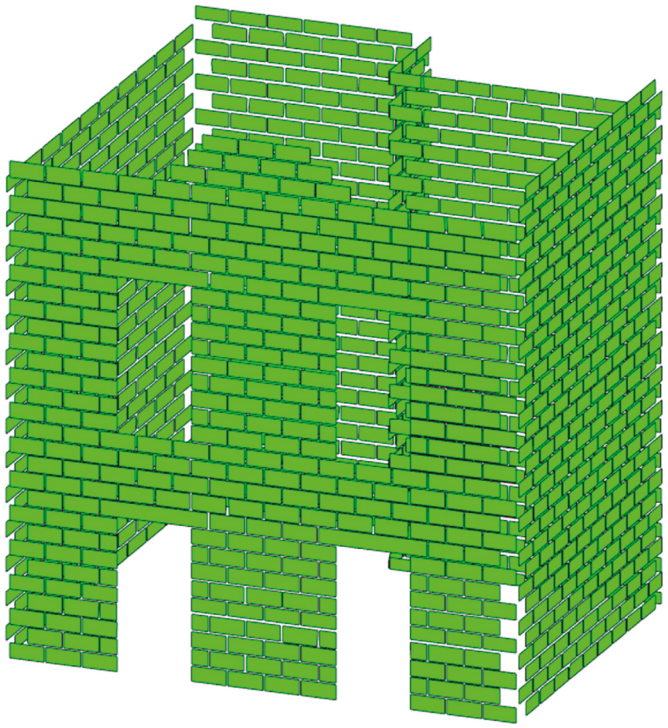

Fig. 11. The outer wall surfaces of the example single-wythe masonry structure with the small corner bricks removed for modeling of structural interlocking between walls.

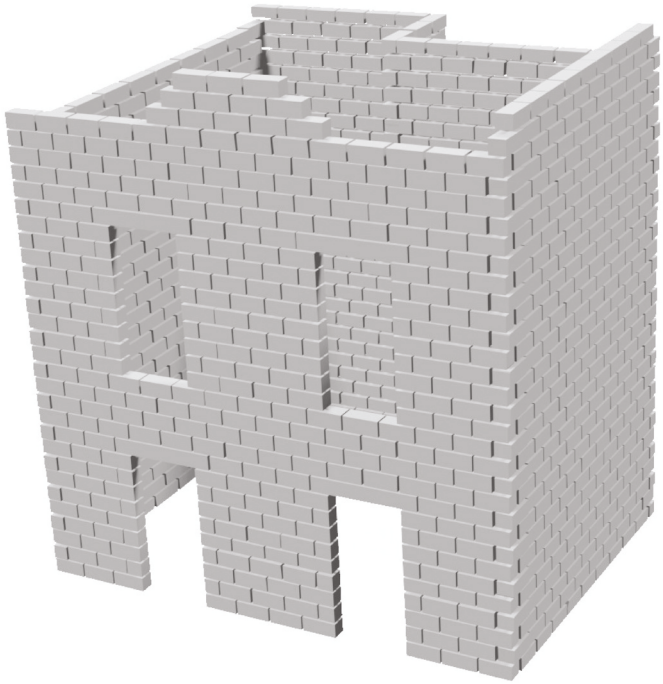

Fig. 12. The developed 3D masonry structure with brick polyhedrons.

The brick shapes are overall rectangular with some variations. We measured the thickness of bricks, which ranges from 378 to 432 mm. For simplicity, all bricks are assumed to have the same thickness of 400 mm. One photo is taken for each side of the structure. These photos are taken at a standing human height, therefore there is perspective-related image distortion in the photos. Adobe Photoshop [57] is adopted to correct the image distortion, for which the perspective wrapping function is used. This function adjusts objects in an image by taking into account the surrounding environment for a pseudo-orthogonal projection. Fig. 14b shows images of all four walls of Stylite Tower after correcting the distortion. It is worth mentioning that the minor visual obstruction (i.e., the steel fence around the structure), as shown in Fig. 14, is also removed using Adobe Photoshop using the content-aware fill function [58].

The segmented and extracted geometries of all bricks are shown in Fig. 15, where the boundaries of each brick are clearly identified and captured. Many bricks in the structure are overall rectangular but have variations, therefore more than 4 vertices are needed to create a high-fidelity wall model. The Dice Similarity Coefficient (DSC), also known as Sørensen–Dice coefficient, is adopted to find the least number of vertices required to represent brick shapes with high accuracy. Developed by Sørensen [59,60]; DSC measures the similarity of two shapes in the range between 0 and 1, where 1 means that the two shapes match perfectly. The DSC is formulated as shown in Eq. (5), where it compares the area of intersection between the brick's original shape ($A_{original}$) and the approximated polygon ($A_{approximated}$) to the sum of the two areas. The approximation of all bricks as 8-sided polygons yields an average DSC value of 0.9845, which strongly suggests that the approximated polygon shapes maintain a high level of geometric accuracy. Fig. 16 shows the approximated polygons of the bricks in all images. Table 3 presents the input parameters used for the image-based modeling of Stylite Tower.

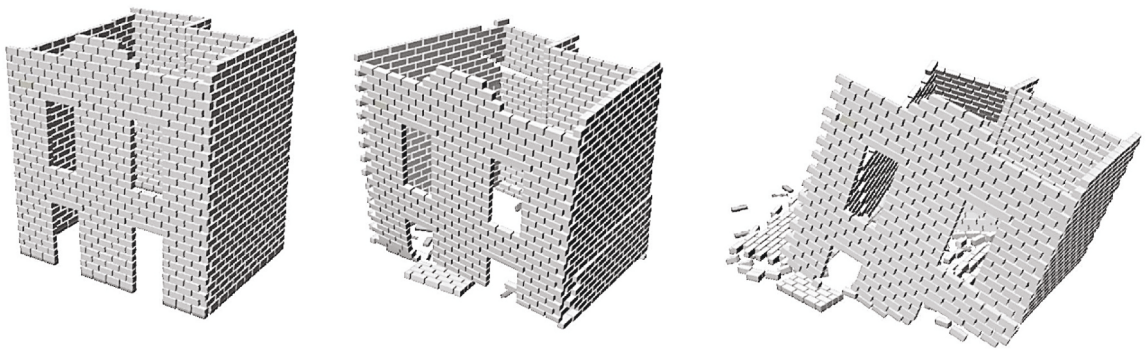

Fig. 13. Collapse simulation of the example single-wythe masonry structure.

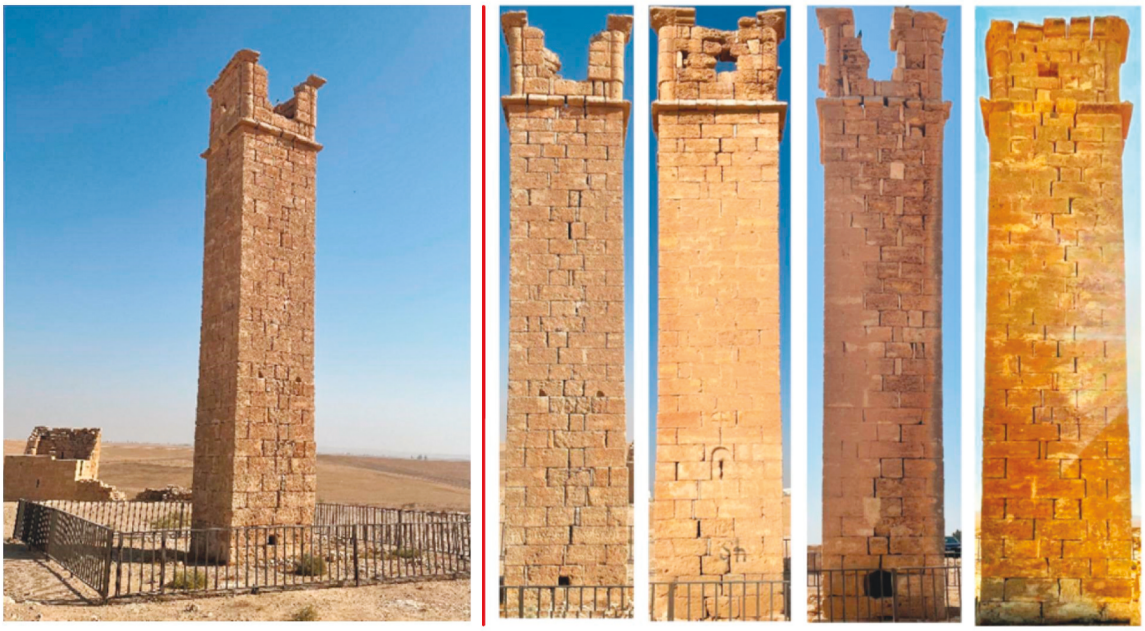

Fig. 14. A heritage single-wythe masonry structure: (a) Stylite Tower in Jordan, (b) Image of each wall of the structure after image distortion corrected (images by Mohammad Abu-Haifa).

$$DSC = \frac{2\left|A_{original} \cap A_{approximated}\right|}{\left|A_{original}\right| + \left|A_{approximated}\right|} \tag{5}$$

The vertices of the simplified polygons are scaled based on the actual dimensions of the structure. The 3D model is then developed with consideration of the stretcher bond. The model is exported to Blender in STL format for DEM simulation. The entire process, which includes building the 3D DEM model of Stylite Tower from the binary images and exporting the model in the required format, takes less than 20 s. A DEM simulation is conducted on the developed Stylite Tower model, following the assignments of material properties, brick constraints, breaking thresholds, and the seismic load. Fig. 17 shows the collapsing sequence of Stylite Tower after applying a synthetic earthquake of magnitude 7 for 10 s. An ordinary computer system running on a 64-bit Windows 11 operating system is used for the simulation. The computer is equipped with a 3 GHz Intel Core i7-9700 processor and 24 GB of RAM. The simulation process runs for approximately 2 min in batch mode.

Previous studies have utilized the finite element method to assess the tower's capacity to withstand seismic events. While these studies highlighted the possibility of collapse if an intense seismic event were to occur in the area, the actual collapse was not simulated due to the limitations of the adopted simulation method [56,61–63]. In contrast, our approach explicitly simulates the potential collapse in response to the given earthquake. It is worth noting that the mechanical properties used in the simulation (including brick and mortar properties) may not represent the actual properties of Stylite Tower. This study focuses on the development of the framework that streamlines the process from 2D imaging to 3D modeling (i.e., via reverse descriptive geometry) and extends it to the DEM simulation. The determination of the actual mechanical properties of the tower is beyond the scope and suggested for future study.

4. Concluding remarks

This paper presents an image-based 3D modeling-to-simulation framework for assessing the hazard vulnerability of single-wythe masonry structures. A 'reverse descriptive geometry' concept is used for 2D-to-3D modeling, whereby a set of 2D images of planar walls are used as an input for 3D modeling of the single-wythe masonry structures, followed by numerical simulation using the discrete element method (DEM). The 2D modeling stage involves the representation of all walls by segmenting and approximating each brick into simplified polygons. The framework then systematically builds the whole 3D structure DEM model from the 2D walls. The adjoining wythes at the building corners are modeled via an original bespoke method proposed in this study. The proposed framework is successfully applied to Stylite Tower, a heritage single-wythe masonry structure in Jordan. The results clearly showcased the applicability of the developed methodology, highlighting the streamlined process for assessing the vulnerability of single-wythe masonry structures. This study pioneers the seamless integration of 2D image processing techniques, 3D modeling, and the impulse-based dynamic simulation (for discrete element analysis), by which it introduces a novel streamlined image-based 3D modeling-to-simulation framework specifically tailored for single-wythe masonry structures. The new contribution is enabled by the

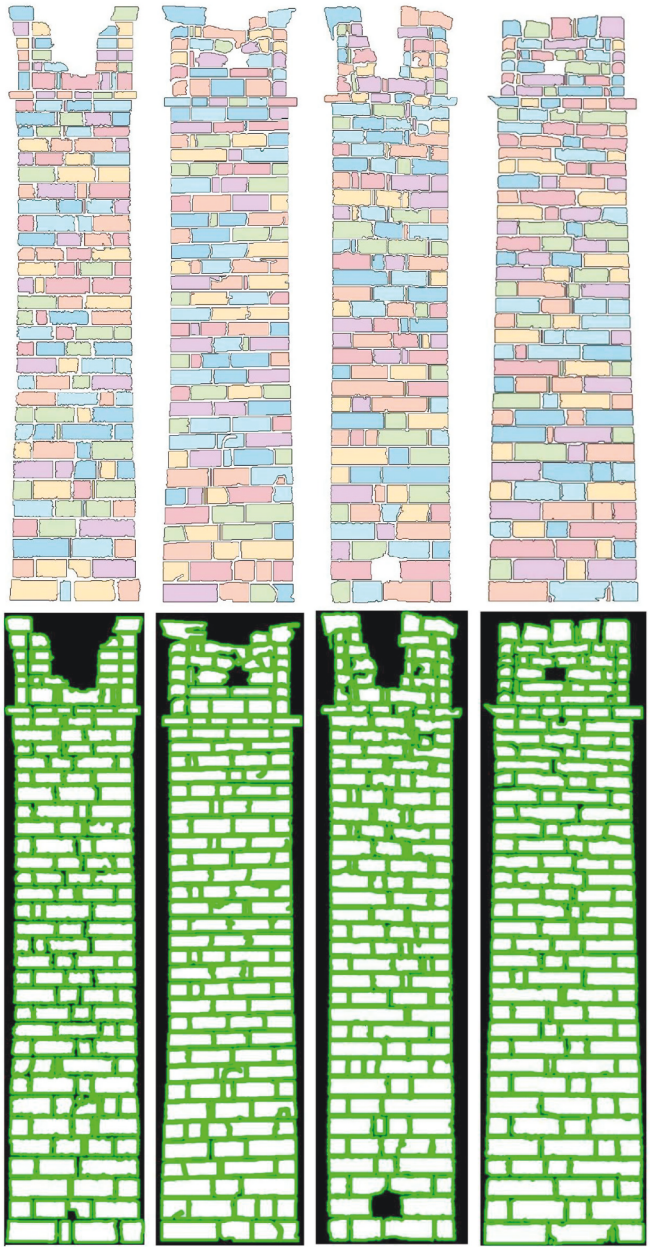

Fig. 15. The segmented images and extracted brick geometries in Stylite Tower.

proposed 'reverse descriptive geometry' concept for 2D-to-3D modeling to digitally build a 3D single-wythe masonry structure model from 2D wall images. This innovative approach presents a significant advancement in the field, offering a highly efficient and effective methodology for analyzing and simulating single-wythe masonry structures. While the focus of this study is on the walls of single-wythe masonry structures, the slab and roof may be easily added to the structure in future studies. The outcomes of this study will offer insight and serve as a foundation for future advancements in the field of masonry structure research. The practical implementation of this research is of great importance, as it has the potential to transform the way masonry structures are analyzed and maintained. We invite the research community to explore the potential of the proposed approach further with various single-wythe structures. The proposed framework may also be extended for multi-wythe masonry structures and complex brick shapes.

Author contributions

Mohammad Abu-Haifa: Conceptualization, Investigation, Software, Visualization, Writing - Original draft, Seung Jae Lee: Funding acquisition, Conceptualization, Methodology, Supervision, Validation, Writing - Review and Editing.

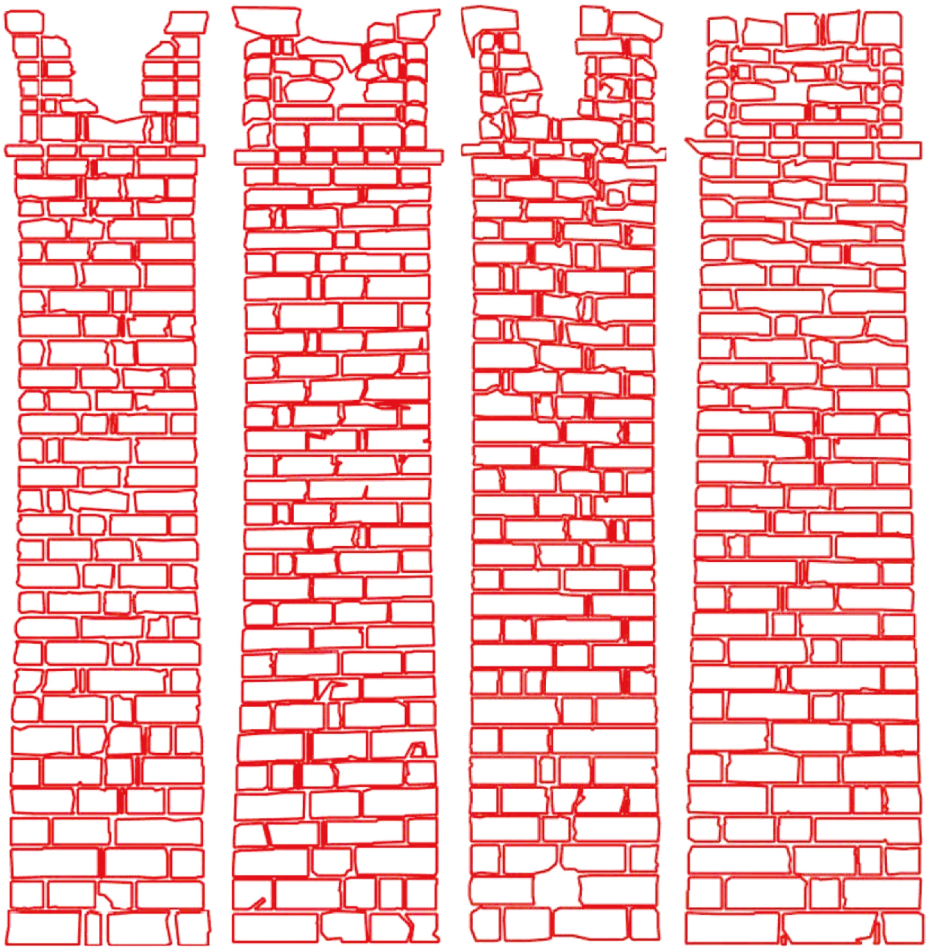

Fig. 16. Simplified polygons with 8 vertices after applying the splitting method on the input images.

Table 3
Input parameters for the image-based modeling of Stylite Tower.

Wall				Brick thickness (m)	Target number of vertices
Image #	Width W (m)	Height H (m)	Orientation θ (°)		
1	2.43	13.5	0	0.40	8
2	2.48	13.5	90	0.40	8
3	2.43	13.5	180	0.40	8
4	2.48	13.5	270	0.40	8

Funding

Seung Jae Lee reports financial support was provided by US National Park Service. Seung Jae Lee reports financial support was provided by US National Science Foundation.

Declaration of competing interest

The authors declare that they have no known competing financial interests or personal relationships that could have appeared to influence the work reported in this paper.

Data availability

Data will be made available on request.

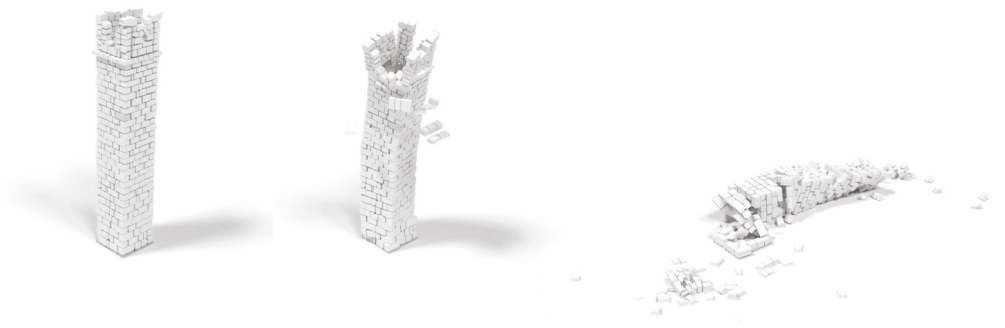

Fig. 17. The 3D DEM simulation for Stylite Tower after applying a synthetic earthquake of magnitude 7 Richter.

Acknowledgements

This work was supported in part by Florida International University's Doctoral Evidence Acquisition (DEA) Fellowship, the National Center for Preservation Technology and Training of the US National Park Service under award P19AP00141, and the US National Science Foundation under award 1635378. The opinions, findings, conclusions, or recommendations expressed in this article are solely those of the authors and do not represent the opinions of the funding agencies.

Glossary

Symbols

FEM	Finite element method
DEM	Discrete element method
X	Global X-direction of the structure
Y	Global Y-direction of the structure
Z	Global Z-direction of the structure
θ	The counterclockwise angle between *X*-axis (global) and *x*-axis (local)
w	Image width in pixels
h	Image height in pixels
x	Local x-direction of the image/wall
y	Local y-direction of the image/wall
z	Local z-direction of the image/wall
W	Width of the image/wall in real dimensions
H	Height of the image/wall in real dimensions
n	Image number
DP	Douglas-Peucker
A_{th}	Threshold area for corner brick detection
t	Brick thickness
STL	Stereolithography file format
BCB	Bullet constraints builder
DSC	Dice Similarity Coefficient
$A_{original}$	Area of brick's original shape
$A_{approximated}$	Area of the approximated polygon

References

[1] D. D'Ayala, Assessing the seismic vulnerability of masonry buildings, in: Handbook of Seismic Risk Analysis and Management of Civil Infrastructure Systems, Elsevier, 2013, pp. 334–365.
[2] R.A. Weber, Building Envelope Design Guide—Masonry Wall Systems, Athena Sustainable Materials Institute, 2013. https://www.wbdg.org.
[3] L. Binda, J. Pina-Henriques, A. Anzani, A. Fontana, P.B. Lourenço, A contribution for the understanding of load-transfer mechanisms in multi-leaf masonry walls: testing and modelling, Eng. Struct. 28 (8) (2006) 1132–1148.
[4] R.M. Martin, D.R. Darr, Market responses to the US timber demand-supply situation of the 1990s: implications for sustainable forest management, For. Prod. J. 47 (11/12) (1997) 27.
[5] M.T.R. Jayasinghe, Loadbearing Construction with Local Bricks, 1998.
[6] A. Al-Sakkaf, T. Zayed, A. Bagchi, A sustainability based framework for evaluating the heritage buildings, Int. J. Energy Optim. Eng. 9 (2) (2020) 49–73.
[7] P.B. Lourenço, Computations on historic masonry structures, Prog. Struct. Eng. Mater. 4 (3) (2002) 301–319.

[8] A. Al-Fakih, M.M.A. Wahab, B.S. Mohammed, M.S. Liew, N.A.W.A. Zawawi, S. As' ad, Experimental study on axial compressive behavior of rubberized interlocking masonry walls, J. Build. Eng. 29 (2020), 101107.
[9] A.C. Altunışık, F. Önalan, F. Sunca, Experimental, numerical and analytical investigation on blast response of brick walls subjected to TNT explosive, J. Struct. Eng. 4 (1) (2021) 28–45.
[10] R.M. Azzara, M. Girardi, V. Iafolla, D.M. Lucchesi, C. Padovani, D. Pellegrini, Ambient vibrations of age-old masonry towers: results of long-term dynamic monitoring in the historic centre of Lucca, Int. J. Architect. Herit. 15 (1) (2021) 5–21.
[11] S. Banerjee, S. Nayak, S. Das, Adjudging efficacy of geonet reinforcement on the seismic performance of brick masonry structures: an experimental study, Mater. Struct. 54 (6) (2021) 1–24.
[12] R. Cacciotti, Brick masonry response to wind driven rain, Eng. Struct. 204 (2020), 110080.
[13] J.M. Pereira, J. Campos, P.B. Lourenço, Masonry infill walls under blast loading using confined underwater blast wave generators (WBWG), Eng. Struct. 92 (2015) 69–83.
[14] G. Vasconcelos, P.B. Lourenço, Experimental characterization of stone masonry in shear and compression, Construct. Build. Mater. 23 (11) (2009) 3337–3345.
[15] G. Zini, M. Betti, G. Bartoli, Experimental analysis of the traffic-induced-vibration on an ancient lodge, Struct. Control Health Monit. 29 (3) (2022), e2900.
[16] T.T. Bui, A. Limam, V. Sarhosis, Failure analysis of masonry wall panels subjected to in-plane and out-of-plane loading using the discrete element method, Eur. J. Environ. Civil Eng. 25 (5) (2019) 876–892.
[17] O.M. Kayırga, F. Altun, Investigation of earthquake behavior of unreinforced masonry buildings having different opening sizes: experimental studies and numerical simulation, J. Build. Eng. 40 (2021), 102666.
[18] D. Malomo, R. Pinho, A. Penna, Numerical modelling of the out-of-plane response of full-scale brick masonry prototypes subjected to incremental dynamic shake-table tests, Eng. Struct. 209 (2020), 110298.
[19] J.V. Lemos, Discrete element modeling of masonry structures, Int. J. Architect. Herit. 1 (2) (2007) 190–213.
[20] H. Smoljanović, N. Živaljić, Ž. Nikolić, A combined finite-discrete element analysis of dry stone masonry structures, Eng. Struct. 52 (2013) 89–100.
[21] T.T. Bui, A. Limam, V. Sarhosis, M. Hjiaj, Discrete element modelling of the in-plane and out-of-plane behaviour of dry-joint masonry wall constructions, Eng. Struct. 136 (2017) 277–294, https://doi.org/10.1016/j.engstruct.2017.01.020.
[22] I. Caliò, M. Marletta, B. Pantò, A new discrete element model for the evaluation of the seismic behaviour of unreinforced masonry buildings, Eng. Struct. 40 (2012) 327–338.
[23] X. Chen, X. Wang, H. Wang, A.K. Agrawal, A.H.C. Chan, Y. Cheng, Simulating the failure of masonry walls subjected to support settlement with the combined finite-discrete element method, J. Build. Eng. 43 (2021), 102558.
[24] A. Dell'Endice, A. Iannuzzo, M.J. DeJong, T. Van Mele, P. Block, Modelling imperfections in unreinforced masonry structures: discrete element simulations and scale model experiments of a pavilion vault, Eng. Struct. 228 (2021), 111499, https://doi.org/10.1016/j.engstruct.2020.111499.
[25] F. Gobbin, G. de Felice, J.V. Lemos, Numerical procedures for the analysis of collapse mechanisms of masonry structures using discrete element modelling, Eng. Struct. 246 (2021), 113047.
[26] N. Kassotakis, V. Sarhosis, B. Riveiro, B. Conde, A.M. D'Altri, J. Mills, G. Milani, S. de Miranda, G. Castellazzi, Three-dimensional discrete element modelling of rubble masonry structures from dense point clouds, Autom. Construct. 119 (2020), 103365.
[27] D. Malomo, M.J. DeJong, A. Penna, Distinct element modelling of the in-plane cyclic response of URM walls subjected to shear-compression, Earthq. Eng. Struct. Dynam. 48 (12) (2019) 1322–1344, https://doi.org/10.1002/eqe.3178.
[28] F. Masi, I. Stefanou, V. Maffi-Berthier, P. Vannucci, A Discrete Element Method based-approach for arched masonry structures under blast loads, Eng. Struct. 216 (2020), 110721, https://doi.org/10.1016/j.engstruct.2020.110721.
[29] G. Occhipinti, I. Caliò, A.M. D'Altri, N. Grillanda, S. de Miranda, G. Milani, E. Spacone, Nonlinear finite and discrete element simulations of multi-storey masonry walls, Bull. Earthq. Eng. 20 (4) (2022) 2219–2244.
[30] B. Pulatsu, E. Erdogmus, E.M. Bretas, Parametric study on masonry arches using 2D discrete-element modeling, J. Architect. Eng. 24 (2) (2018), 04018005, https://doi.org/10.1061/(ASCE)AE.1943-5568.0000305.
[31] M. Abu-Haifa, S.J. Lee, Image-based modeling-to-simulation of masonry walls, J. Architect. Eng. 28 (4) (2022), 06022001, https://doi.org/10.1061/(ASCE)AE.1943-5568.0000569.
[32] G. Castellazzi, A. D'Altri, G. Bitelli, I. Selvaggi, A. Lambertini, From laser scanning to finite element analysis of complex buildings by using a semi-automatic procedure, Sensors 15 (8) (2015) 18360–18380, https://doi.org/10.3390/s150818360.
[33] M. Ioannides, D. Fritsch, J. Leissner, R. Davies, F. Remondino, R. Caffo, in: Progress in Cultural Heritage Preservation: 4th International Conference, EuroMed 2012, Lemessos, Cyprus, October 29–November 3, 2012, Proceedings, vol. 7616, Springer Science & Business Media, 2012.
[34] D. Loverdos, V. Sarhosis, E. Adamopoulos, A. Drougkas, An innovative image processing-based framework for the numerical modelling of cracked masonry structures, Autom. Construct. 125 (2021), 103633.
[35] F. Micelli, A. Cascardi, Structural assessment and seismic analysis of a 14th century masonry tower, Eng. Fail. Anal. 107 (2020), 104198.
[36] L. Truong-Hong, D.F. Laefer, T. Hinks, H. Carr, Combining an angle criterion with voxelization and the flying voxel method in reconstructing building models from LiDAR data, Comput. Aided Civ. Infrastruct. Eng. 28 (2) (2013) 112–129.
[37] R. Migliari, Descriptive geometry: from its past to its future, Nexus Netw. J. 14 (3) (2012) 555–571.
[38] MathWorks, MATLAB R2021a (Ver. R2021a), 2021.
[39] The Blender Foundation, Blender – a 3D Modelling and Rendering Package (2.75), http://www.blender.org, 2021.
[40] E. Coumans, Bull. Phys. 3 (17) (2020).
[41] C.E. Augarde, S.J. Lee, D. Loukidis, Numerical modelling of large deformation problems in geotechnical engineering: a state-of-the-art review, Soils Found. 61 (6) (2021) 1718–1735, https://doi.org/10.1016/j.sandf.2021.08.007.
[42] S. Smith, Bonding, in: Brickwork, Springer, 1972, pp. 15–25.
[43] R. Bärtschi, T. Bonwetsch, A stretcher bond with defects applied to a hyperboloid, in: Advances in Architectural Geometry 2012, Springer, 2013, pp. 37–42.
[44] H.-D. Cheng, X.H. Jiang, Y. Sun, J. Wang, Color image segmentation: advances and prospects, Pattern Recogn. 34 (12) (2001) 2259–2281.
[45] Y. Ibrahim, B. Nagy, C. Benedek, CNN-based watershed marker extraction for brick segmentation in masonry walls, Int. Conf. on Image Anal. Recogn. (2019) 332–344.
[46] B. Riveiro, P.B. Lourenço, D.V. Oliveira, H. González-Jorge, P. Arias, Automatic morphologic analysis of quasi-periodic masonry walls from LiDAR, Comput. Aided Civ. Infrastruct. Eng. 31 (4) (2016) 305–319, https://doi.org/10.1111/mice.12145.
[47] E. Valero, F. Bosché, A. Forster, Automatic segmentation of 3D point clouds of rubble masonry walls, and its application to building surveying, repair and maintenance, Autom. ConStruct. 96 (2018) 29–39.
[48] MathWorks, Trace Region Boundaries in Binary Image - MATLAB Bwboundaries. https://www.mathworks.com/help/images/ref/bwboundaries.html, 2023.
[49] A. Pikaz, I. hak Dinstein, An algorithm for polygonal approximation based on iterative point elimination, Pattern Recogn. Lett. 16 (6) (1995) 557–563.
[50] B. Lelandais, I. Gardin, L. Mouchard, P. Vera, S. Ruan, Dealing with uncertainty and imprecision in image segmentation using belief function theory, Int. J. Approx. Reason. 55 (1) (2014) 376–387.
[51] P. Bone, Polygon simplification, MATLAB Central File Exchange, https://www.mathworks.com/matlabcentral/fileexchange/45342-polygon-simplification, 2023.
[52] S.G. Pauker, J.P. Kassirer, The threshold approach to clinical decision making, N. Engl. J. Med. 302 (20) (1980) 1109–1117, https://doi.org/10.1056/NEJM198005153022003.
[53] P.A. Cundall, R.D. Hart, Numerical modelling of discontinua, Eng. Comput. 9 (2) (1992) 101–113, https://doi.org/10.1108/eb023851.
[54] K. Kostack, Bullet Constraints Builder for Blender. https://github.com/KaiKostack/bullet-constraints-builder, 2021.
[55] S.J. Lee, Y.M.A. Hashash, iDEM: an impulse-based discrete element method for fast granular dynamics, Int. J. Numer. Methods Eng. 104 (2) (2015) 79–103, https://doi.org/10.1002/nme.4923.

[56] P. Clemente, G. Delmonaco, L. Puzzilli, F. Saitta, Seismic analysis of the stylite tower at Umm ar-Rasas, in: Structural Analysis of Historical Constructions, Springer, 2019, pp. 1780–1788.
[57] Adobe Photoshop, Adobe Photoshop (version 24.0.0), Preuzeto, 2022, 2022.
[58] Adobe Photoshop, Remove objects from Your Photos with Content-Aware Fill. Adobe. https://helpx.adobe.com/photoshop/using/content-aware-fill.html, 2022.
[59] T.A. Sorensen, A method of establishing groups of equal amplitude in plant sociology based on similarity of species content and its application to analyses of the vegetation on Danish commons, Biol. Skar. 5 (1948) 1–34.
[60] L.R. Dice, Measures of the amount of ecologic association between species, Ecology 26 (3) (1945) 297–302.
[61] P. Clemente, G. Delmonaco, L. Puzzilli, F. Saitta, Stability and seismic vulnerability of the stylite tower at Umm ar-Rasas, Ann. Geophys. 62 (3) (2019).
[62] W. Koellisch, Umm er Rasas, a World Heritage site, mysterious and hidden. Preventive measures against damage from earthquakes and heavy rains, Heritage Risk (2008) 73–77.
[63] R. Pierdicca, C. Intrigila, F. Piccinini, E.S. Malinverni, I. Giannetti, G. Caruso, Multidisciplinary approach for the analysis of structural heritage at risk: the case study of stylite tower at Umm ar-Rasas (Jordan), Int. J. Architect. Herit. (2021) 1–25.